Performance analysis of wave energy resources at a WEC test site in Keelung, Taiwan

S. Y. Tzang, Y. L. Chen, H. Z. Chen, J. H. Chen, Y. H. Lee, and Y. C. Chow

Abstract—**From wave data of a buoy at a test site offshore Keelung of Taiwan, 16 cases with wave periods ranging from 7-11 s for top annual energy potentials were selected. They consist of 55% of total occurrence probability and 74% of total annual energy potentials. Peak occurrence probabilities and annual energy potentials are found to be due to waves with heights less than 1 m and of 1.5-3.5 m while periods of 5-7 s and of 8-10 s, respectively. The wave energy characteristics were further applied to performance analysis for a laboratory model gravity-type OWC. A 1D OWC time-domain model without PTO was adopted for simulating performance of wave energy capturing. The numerical model was first validated by experimental measurements for an OWC in a water depth of 0.5 m. Better agreements were found for smaller and shorter waves. The JONSWAP-type irregular waves with the same peak enhancement factor γ =1.7 of the 16 cases were then adopted in the 1D modelling for the same laboratory OWC model. The simulations demonstrated capture factor CF ranging from 32% to 40 %. Better capture performances were due to cases with top annual energy potentials with wave periods of about 9 s. In other cases, shorter waves would result in higher CF than longer waves. Thus, for designing an optimized wave energy converter WEC in wave energy resources similar to those in present test site, performance analysis can be first carried out by adopting the selected wave conditions for a typical WEC model.**

Keywords—**wave energy resources, WEC test site, performance analysis, 1D OWC model, irregular waves.**

I. Introduction

In Taiwan, one of the prior marine energy resources is wave energy and higher potentials in coastal waters are concluded to be located in the northeast (NE) Taiwan [1]. Thus, to facilitate the development of the wave energy conversion technology, a permitted field test site was established in 2011 offshore Keelung in northeast Taiwan. A wave data buoy was then installed on the offshore boundary of the test site since 2012 to continually collect wave information entering the test site. Reference [2] reported the analysis of collected waves for three years from May 2012 to May 2015. They found from results of joint probability distributions of wave heights and periods and monthly variations of averaged wave energy resources that waves are larger and longer resulting in higher wave energy potential especially in the Northeast Monsoon season (Oct. to next March). Chien & Kuo [3] had found that the characteristic wave spectrum for relatively larger waves around NE coastal waters followed standard JONSWAP type with a typical value of peak enhancement factor γ =1.7. To demonstrate the characteristics of these in-situ wave energy resources for a specific wave energy conversion system, a most popular OWC was adopted for performance analysis. In this study, 16 studied cases were first selected from the power scatter diagram based on rankings of annual energy production and occurrence probabilities as proposed by [4]. Then a 1D time-domain OWC model by [5] was used for giving in the chamber the details of the water surface variations, air flow rate, air pressure drop and pneumatic power. Numerical simulations for a laboratory model OWC (Lee, et al.) was first validated with the experimental measurements. Then, irregular wave-induced performance for the selected 16 cases were calculated and analysed.

Paper ID number:1560- Conference track: WRC

S. Y. Tzang, H. Z. Chen, J. H. Chen, Y. H. Lee, Y. C. Chow are with the Center for Ocean Energy System, National Taiwan Ocean University, 2nd Pei-Ning Rd, Keelung, 212, Taiwan, ROC (e-mail: sytzang@ntou.edu.tw).

Y. L. Chen was with Research Center for Ocean Energy and Strategy, National Taiwan Ocean University. He is now with Minesto Taiwan Ltd. 24F, No. 333 Keelung Rd. Sec. 1, Taipei 11012, Taiwan, ROC (e-mail: yunglung.chen@minesto.com).

II. Wave Energy Resources Characteristics

The wave height and power scatter diagrams by [2] from field measurements by a data buoy during May 2012 to May 2015 were first processed for test cases in present study. As shown in Fig. 1 & Fig. 2, the probabilities have been substituted by hours in each bin. The magnitudes are represented by colour bars on the sides. Based on the sorting of the annual energy potentials from highest to lowest within combined four bins in the diagram resulted in 16 cases, entitled with J01 to J16. The selected 16 cases (J01 to J16) consist of only 55% of total occurrence probability but amount to 74% of total annual energy potentials per meter. It is clearly noted in Figure 1 that

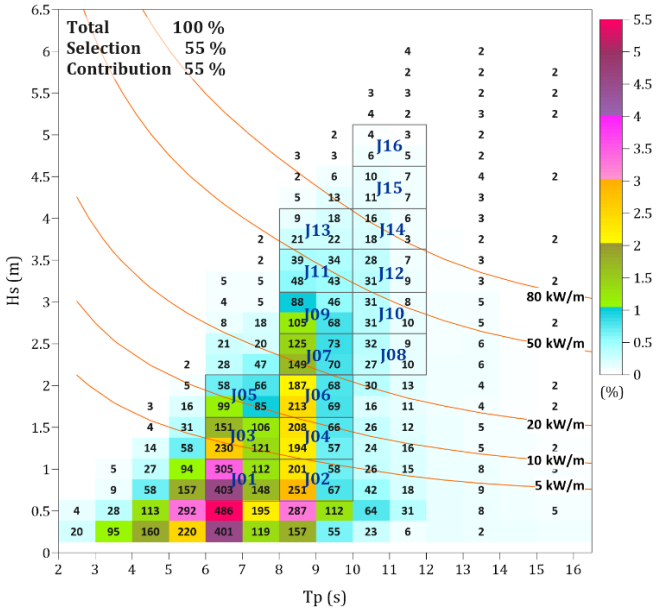

Fig. 1. Typical joint probability distribution of H & T.

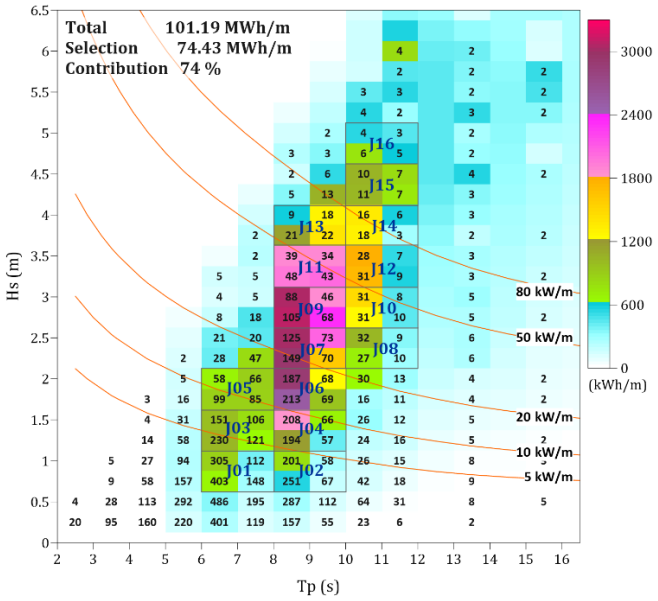

Fig. 2. Annual energy potentials corresponding to the sea states.

peak occurrence probabilities greater than 4% are mainly due to waves with heights less than 1 m and periods of 5-7 s. In Figure 2, the peak annual energy potentials greater than 1800 kWh/m are due to larger and longer waves with heights 1.5-3.5 m and periods of 8-10 s.

III. 1D OWC MODEL

The 1D time-domain OWC model [5] was adopted in this paper. The hydrodynamic force is coupled with the thermodynamic force for an OWC system with an orifice. Some assumptions are made in the mathematical model. The linear wave theory is used to simulate components of the irregular waves while wave diffraction being neglected. The incident wave field is assumed incompressible and irrotational. In addition, vortex and viscous effects inside the air chamber are not considered either. Finally, the air is assumed incompressible and the

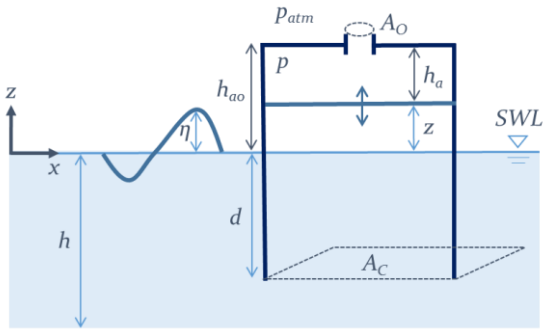

Fig. 3. Schematic representation of the OWC model.

air density through the orifice plate is constant due to small chamber in size.

The pneumatic power generated in the OWC is a function of the inner free surface elevation $z(t)$ and air chamber pressure drop $\Delta p(t)$. Fig. 3 shows a schematic representation of an OWC. Based on Newton's second law, the motion of internal water volume can be formulated as the total forces with respect to time, $F(t)$, which is given by (1),

$$M\ddot{z} + B\dot{z} + Cz = F(t) \tag{1}$$

$$\begin{cases} M = \rho_w A_C \cdot (d + z) \\ B = 0.2 \cdot \sqrt{C(M + M_a)} \\ C = \rho_w g A_C \\ M_a = \dfrac{2}{3}\sqrt{\dfrac{A_C}{\pi}} \end{cases} \tag{2}$$

where M is the water column mass, B the damping coefficient and C the hydrostatic restoring coefficient. The above coefficients can be derived from (2) where M_a is the added mass, ρ_w is water density, d is the draft and A_C the air chamber area. The total forces, as shown in (3), that acts on the water column can be expressed as the excitation forces including the added mass force $F_a(t)$, the Froude-Krylov force $F_{FK}(t)$ and the force due to varying air pressure $F_{\Delta pair}(t)$, which

$$F(t) = F_a(t) + F_{KT}(t) + F_{\Delta p_{air}}(t) \tag{3}$$

The added mass force $F_a(t)$ depends on the difference between vertical water particle velocity and acceleration of the water column:

$$F_a(t) = M_a \cdot (\dot{w} - \ddot{z}) \tag{4}$$

where $\dot{w}$ is the water particle acceleration. The Froude-Krylov force $F_{FK}(t)$ is created by the wave hydrodynamic pressure acting on the bottom of the water column, can be expressed by (5).

$$F_{KT}(t) = p_{wave}(t) \cdot A_C \tag{5}$$

The air force is defined as (6), where Δp is the difference between the internal chamber pressure and the atmospheric pressure.

$$F_{\Delta p_{air}}(t) = -\Delta p \cdot A_C \tag{6}$$

The water surface displacement η(t) varies sinusoidally with respect to time, and is a function of amplitude a_i, angular frequency ω_i and phase φ_i as given in:

$$\eta_i(t) = a_i \cdot \cos(\omega_i t + \phi_i) \tag{7}$$

The water particle acceleration at arbitrary depth z is described as:

$$\dot{w}_i(t) = -\omega_i^2 a_i \cdot \frac{sinhk_i(z+h)}{sinhk_i h} \cdot \cos(\omega_i t + \phi_i) \tag{8}$$

The wave hydrodynamic pressure at depth d is determined by

$$p_{wave_i}(t) = \rho g a_i \frac{coshk_i(h-d)}{coshk_i h} \cos(\omega_i t + \phi_i) \tag{9}$$

Therefore, the equation of motion of water column forced by irregular waves can be rewritten as (10), in which α and β_i can be derived by (11). According to the ideal gas law, the governing equation of the pressure inside the chamber can be determined, as given in (10).

$$\begin{cases} \ddot{z} = -0.2\sqrt{\dfrac{g}{\alpha+z}}\dot{z} - \dfrac{g}{\alpha+z}z \\ \quad + \dfrac{1}{\alpha+z}\displaystyle\sum_{i-1}^{N}\beta_i a_i cos\,(\omega_i t + \phi_i) - \dfrac{\Delta p}{\rho_w(\alpha+z)} \\ \Delta\dot{p} = \dfrac{-c_s^2 C_d A_O}{A_C(h_{a0}-z)}\sqrt{2\Delta p \cdot \rho_a} + \gamma\dfrac{(\Delta p + p_{atm})\dot{z}}{h_{a0}-z} \end{cases} \tag{10}$$

$$\begin{cases} \alpha = d + \dfrac{2}{3}\sqrt{\dfrac{A_C}{\pi}} \\ \beta_i = g\dfrac{coshk_i(h-d)}{coshk_i h} - \dfrac{2}{3}\sqrt{\dfrac{A_C}{\pi}} \cdot \omega_i^2 \dfrac{sinhk_i(h-d)}{sinhk_i h} \end{cases} \tag{11}$$

IV. VALIDATIONS AND PERFORMANCE ANALYSIS

Heights of the displacing water surface in the chamber of an OWC were calculated by the 1D model. Numerical simulations were first validated by experimental flume measurements with schematic configurations similar to that of Fig. 1 by [6]. Four of their tests including wave conditions and wave heights in the chamber H_{owc} were selected and listed in Table I. The comparisons of H_{owc} between measurements and model simulations were illustrated in Fig. 4. The comparisons have shown that

TABLE I
WAVE TANK TEST CONDITIONS SELECTED FOR NUMERICAL MODEL VALIDATION

Test Run	H [cm]	T [s]	H_{OWC} [cm]
1	7.27	1.56	10.25
2	10.59	1.56	12.51
3	6.87	2.00	8.67
4	9.05	2.00	11.42

TABLE II
SIMULATION RESULTS OF THE TANK TEST CONDITIONS

Test Run	H (cm)	T (s)	L (m)	h/L -	Pw (W)	Q (m3/s)	Δp (Pa)	Pn (W)	CF (%)
1	7.26	1.56	2.98	0.17	3.00	0.011	98.91	1.47	49.19
2	10.57	1.56	2.98	0.17	6.36	0.014	158.67	2.99	46.99
3	6.86	2.00	4.06	0.12	3.16	0.010	71.48	0.90	28.49
4	9.04	2.00	4.06	0.12	5.49	0.012	111.23	1.74	31.74

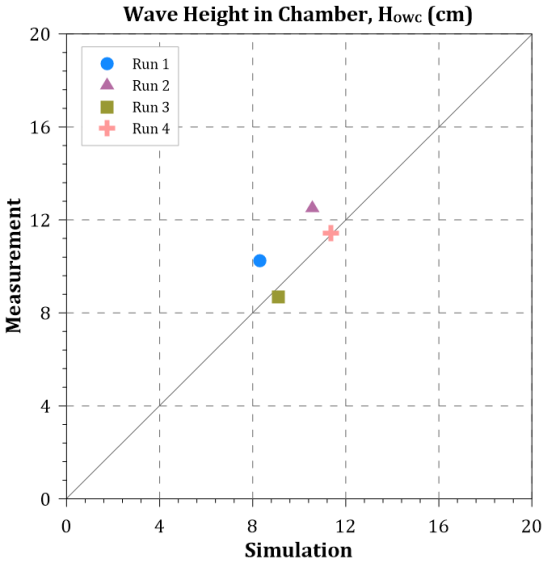

Fig. 4. Comparisons of wave height between measurements and model simulations.

simulations of test runs with wave period of 2 s (i.e. Run 3 & 4) are in better agreements with experimental measurements than those for test runs with period of 1.56 s (i.e. Run 1 & 2). On the other hand, the simulated values of resulting capture factor CF, as shown in Table II, are much higher for Test Runs 1 & 2 implying smaller and shorter waves in a fixed water depth would give better performance for a gravity-type OWC based on 1D modelling with linear waves.

Subsequently, the 1D model was further applied to simulate capture performance with irregular waves. For simulations in a similar model water depth of 0.5 m, the OWC was assumed to be deployed in a field water depth of 15m so that the model length scale would be 1/30. Disregarding the shallow water effects from 40 m to 15 m, the derived scatter diagram in Fig. 3 & Fig. 4 are directly applied for the water depth of 15 m. Thus, for each of the selected 16 cases, the wave conditions and corresponding power densities in both field and model scales were listed in Table III. Corresponding spectral characteristics of a JONSWAP type with a common value of peak

TABLE III
SIMULATION RESULTS OF THE SELECTED IRREGULAR WAVE CONDITIONS

Test Run	Model scale (h = 0.5 m)						Full scale (h = 15 m)						CF (%)
	Hs (cm)	Tp (s)	Pw (W)	Q (m^3/s)	Δp (Pa)	Pn (W)	Hs (m)	Tp (s)	Pw (kW)	Q (m^3/s)	Δp (kPa)	Pn (kW)	
J01	2.95	1.27	0.22	0.0038	12.43	0.08	0.89	6.98	33.16	18.60	0.37	11.20	33.77
J02	2.90	1.65	0.27	0.0039	13.20	0.08	0.87	9.04	40.63	19.07	0.40	12.22	30.08
J03	4.63	1.27	0.55	0.0053	24.59	0.21	1.39	6.95	81.43	25.93	0.74	31.09	38.18
J04	4.60	1.68	0.69	0.0057	28.37	0.26	1.38	9.19	102.15	28.24	0.85	37.95	37.15
J05	6.42	1.27	1.09	0.0067	39.48	0.43	1.93	6.96	160.70	33.02	1.18	63.63	39.59
J06	6.23	1.65	1.25	0.0070	42.32	0.47	1.87	9.01	184.96	34.36	1.27	69.70	37.68
J07	7.97	1.67	2.07	0.0083	59.37	0.78	2.39	9.17	305.51	40.81	1.78	115.33	37.75
J08	7.96	2.03	2.27	0.0079	55.41	0.71	2.39	11.10	335.09	39.15	1.66	104.71	31.25
J09	9.68	1.67	2.99	0.0092	72.91	1.06	2.90	9.14	441.75	45.20	2.19	156.85	35.51
J10	9.63	1.95	3.23	0.0092	72.18	1.03	2.89	10.68	477.98	45.18	2.17	152.01	31.80
J11	11.38	1.64	4.08	0.0104	91.46	1.47	3.41	8.96	602.95	51.11	2.74	216.76	35.95
J12	11.28	2.01	4.56	0.0105	92.14	1.46	3.38	11.00	674.13	51.70	2.76	215.40	31.95
J13	13.13	1.65	5.96	0.0116	117.84	2.16	3.94	9.06	881.14	57.39	3.54	319.02	36.21
J14	12.79	2.00	5.90	0.0114	114.11	2.07	3.84	10.95	872.47	56.42	3.42	305.90	35.06
J15	14.89	2.03	8.37	0.0127	137.21	2.69	4.47	11.13	1237.99	62.71	4.12	397.07	32.07
J16	16.45	2.02	9.69	0.0135	153.73	3.15	4.94	11.04	1432.41	66.57	4.61	466.42	32.56

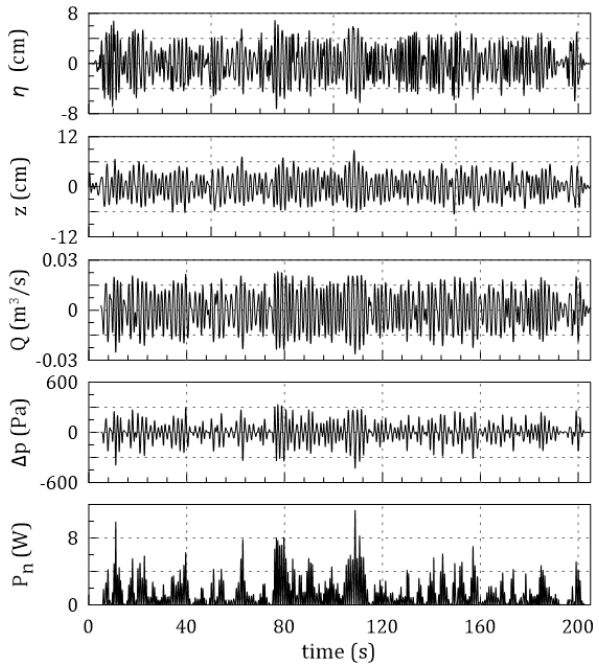

Fig. 5. Time series of (a) Incident wave oscillation, (b) water surface displacement in chamber, (c) air flow rate, (d) air pressure drop and (e) pneumatic power for test run J09.

enhancement factor γ =1.7 were derived and subsequently converted to a time series of water surface displacements with random phases following the Normal Distribution [7]. Fig. 5 demonstrated typical simulated time series of incident wave oscillation, water surface displacement in chamber, air flow rate, air pressure drop and pneumatic power for test run J09. The responses were seen to be almost in phase with the incident wave motions.

Then, the simulated results for all the 16 cases for the model conditions and the converted power results for field conditions were summarized in Table III. It is clearly noted in Table III that the resulting values of CF range from 32 % to 40 % with an average of 34.8%. The highest five cases were associated with J03 to J07 with CF values all higher than 37%. In addition, wave periods of these tests were all around 1.27 s and 1.67 s and most of those with lower CF values were around 2.0 s. In cases of J03 to J07, the results based on 1D model seem to suggest for such an OWC that shorter waves could give better performance with higher CF values, e.g. cases J03 & J05 vs. J04, J06 & J07.

By applying the derived values of CF to the annual energy potential scatter diagram of Fig. 2, we could further evaluate the absorbed energy production for such an OWC in the test site offshore Keelung. The results are summarized in Table IV and Fig. 6, respectively. The simulated results of the selected 16 study cases for the model scales were converted to the field conditions as seen in Table IV. It is clearly seen that both the top highest annual energy potentials and absorbed energy productions all the same occurred in the cases J09, J07, J06 & J11. These four cases have closely similar wave periods of about 9 s with also similar values of CF ranging from 35.5% to 37.8%. They constitute about 48% and 50% of annual potentials and absorbed energy productions, respectively. In addition, the three cases J03-J05 with similar annual potentials and absorbed energy productions constitute similarly 16%-17% of both annual potentials and absorbed productions due to a high averaged value of CF of 38.3%. Though, the four cases J12-J15 constitute 20.3% of annual energy potentials, the absorbed energy production decrease slightly to 19.3% due to lower average CF of 33.8%. It is also noted that the three cases of J03-J05 were associated with wave periods equal or shorter than 9 s, while those of J12-J15 being with periods equal or longer than 9s.

TABLE IV
ANNUAL WAVE ENERGY AND ABSORBED ENERGY FOR THE SELECTED WAVE CASES

Test Run	Hs (m)	Tp (s)	Pw (kW)	Pn (kW)	Prob (%)	Time (hr)	Ew (MWh)	En (MWh)
J01	0.89	6.98	33.16	11.20	11.02	96635	3204.27	1082.15
J02	0.87	9.04	40.63	12.22	6.58	57648	2342.07	704.55
J03	1.39	6.95	81.43	31.09	6.92	60638	4937.99	1885.53
J04	1.38	9.19	102.15	37.95	5.97	52348	5347.45	1986.55
J05	1.93	6.96	160.70	63.63	3.52	30849	4957.51	1962.82
J06	1.87	9.01	184.96	69.70	6.11	53560	9906.21	3732.87
J07	2.39	9.17	305.51	115.33	4.75	41637	12720.45	4801.78
J08	2.39	11.10	335.09	104.71	0.89	7760	2600.12	812.51
J09	2.90	9.14	441.75	156.85	3.50	30660	13543.76	4809.08
J10	2.89	10.68	477.98	152.01	0.92	8100	3871.71	1231.33
J11	3.41	8.96	602.95	216.76	1.87	16390	9882.13	3552.61
J12	3.38	11.00	674.13	215.40	0.86	7570	5103.35	1630.65
J13	3.94	9.06	881.14	319.02	0.80	7003	6170.20	2233.96
J14	3.84	10.95	872.47	305.90	0.50	4353	3797.76	1331.55
J15	4.47	11.13	1237.99	397.07	0.39	3444	4264.24	1367.71
J16	4.94	11.04	1432.41	466.42	0.21	1817	2602.49	847.42

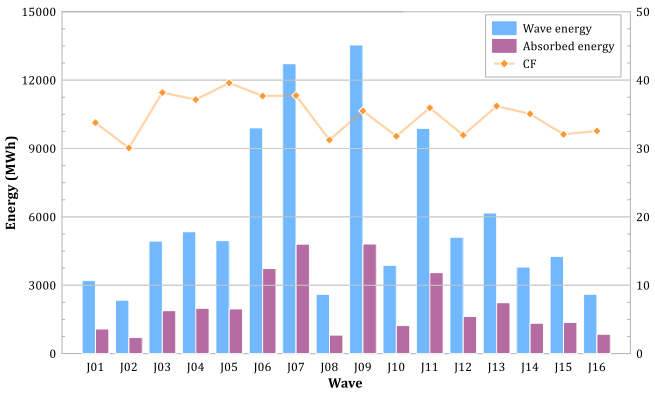

Fig. 6. Annual wave energy potentials, absorbed energy productions and capture factors for the selected wave cases.

V. CONCLUSIONS

By processing the field wave data by a buoy offshore Keelung, Taiwan, 16 study cases with wave periods ranging from 7-11 s with top annual energy productions were selected. The selected 16 cases (J01 to J16) consist of only 55% of total occurrence probability but amount to 74% of total annual energy potentials per meter. The peak occurrence probabilities greater than 4% are mainly due to waves with heights less than 1 m and periods of 5-7 s. But the peak annual energy potentials are due to waves with heights 1.5-3.5 m and periods of 8-10 s. The wave energy characteristics were further applied to the performance analysis for a model gravity-type OWC. An 1D OWC time-domain model without the inclusions of PTO was adopted for simulating the performance of wave energy capturing for the selected cases. The model was first validated by experimental measurements for a model OWC in a flume with a water depth of 0.5 m and better agreements were found typically for smaller and shorter waves. Then JONSWAP-type irregular wave conditions with the same peak enhancement factor γ =1.7 of the 16 cases were adopted in the 1D modelling. The wave conditions for the prototype OWC in the water depth of 15 m were assumed to be the same as those by data buoy and were 1/30 length down-scaled to the laboratory flume model in a water depth of 0.5 m. As a result, the simulations by the 1D model had demonstrated values of capture factor CF ranging from 32% to 40 %. The four cases with top annual energy productions having closely similar wave periods of about 9 s gave better capture performance with an averaged CF of 36.7%. They constitute about 48% and 50% of annual potentials and absorbed energy productions. For the rest of the cases, those with shorter waves were seen to result in higher values of CF than those with longer waves. Thus, for the wave energy characteristics in the waters of the test sites offshore Keelung of Taiwan, better performance for an gravity-type OWC are due to wave periods of about 9 s or 7 s. They are also associated with higher annual wave energy potentials with wave heights ranging from 1.5 to 3.5 m in the test site. The 1D model is indeed limited for practical application, e.g. without PTOs and dimension deficiency, but it serves a quick tool for obtaining a initial satisfactory draft device. That is, for designing an optimized WEC in the wave energy resources similar to those in the test site offshore Keelung, similar scenario of performance analysis can be first carried out by adopting the selected wave conditions for a typical empirical or numerical model.

ACKNOWLEDGEMENT

The authors are grateful for the financial support of Ministry of Science and Technology of Taiwan under the contract No. MOST 107-2221-E-019-055-MY2.

REFERENCES

[1] S.-Y. Tzang, C.-C. Wang, D.-W. Chen, J.-Z. Yang, C.-M. Hsieh, J.-H. Chen, "Wave Energy Resources on Coastal Waters of Northeast Taiwan," in *4th International Conference on Ocean Energy*, 2012, Section. 2-1, No.2.

[2] S.-Y. Tzang, C.-C. Chen, Y.-L. Chen, H.-R. Chen, J.-H. Chen, "Wave Energy Resources at the Test Site in Keelung, Taiwan," in *4th Asian Wave and Tidal Energy Conference*, 2018, Proc. No. 515.

[3] C.-C. Chien and Y.-Y. Kuo, "A Study on the Spectral Form of Nearshore Water Waves," in 16th Conference on Ocean Engineering, 1994, Proc. pp. A193-A215.

[4] I. Lopez, B. Pereiras, F. Castro, G. Iglesias, "Holistic performance analysis and turbine-induced damping for an OWC wave energy converter," *Renewable Energy*, vol. 85, pp. 1155-1163, 2016.

[5] R. Gervelas, F. Trarieux, and M. Patel. "A Time-Domain Simulator for an Oscillating Water Column in Irregular Waves at Model Scale." *Ocean Eng.*, vol. 38, no. 8-9, pp. 1007-1013, 2011.

[6] Y.-H. Lee, Y. Chen, Y.-C. Chow, "Effexts of wave guide plates on the capture factor of the OWC," *Journal of Taiwan Society of Naval Architects and Marine Engineers*, vol. 36, no. 4, 2017.

[7] M. Folley (ed), Numerical Modelling Of Wave Energy Converters, Elsevier, pp. 287, 2016.